HHS Public Access

Author manuscript

Nat Genet. Author manuscript; available in PMC 2014 November 01.

Published in final edited form as:

Nat Genet. 2014 May ; 46(5): 467–473. doi:10.1038/ng.2935.

Genomic and molecular characterization of esophageal squamous cell carcinoma

De-Chen Lin[1,2,8,9], **Jia-Jie Hao**[3,8], **Yasunobu Nagata**[4,8], **Liang Xu**[2,8], **Li Shang**[3], **Xuan Meng**[2], **Yusuke Sato**[4], **Yusuke Okuno**[4], **Ana Maria Varela**[2], **Ling-Wen Ding**[2], **Manoj Garg**[2], **Li-Zhen Liu**[2], **Henry Yang**[2], **Dong Yin**[5], **Zhi-Zhou Shi**[3], **Yan-Yi Jiang**[3], **Wen-Yue Gu**[3], **Ting Gong**[3], **Yu Zhang**[3], **Xin Xu**[3], **Ori Kalid**[6], **Sharon Shacham**[6], **Seishi Ogawa**[4], **Ming-Rong Wang**[3,9], and **H. Phillip Koeffler**[1,2,7]

[1]Cedars-Sinai Medical Center, Division of Hematology/Oncology, UCLA School of Medicine, Los Angeles, USA

[2]Cancer Science Institute of Singapore, National University of Singapore, Singapore

[3]State Key Laboratory of Molecular Oncology, Cancer Institute (Hospital), Peking Union Medical College and Chinese Academy of Medical Sciences, Beijing, China

[4]Cancer Genomics Project, Graduate School of Medicine, The University of Tokyo, Tokyo, Japan

[5]Medical Research Center, Sun Yat-Sen Memorial Hospital, Guangzhou, China

[6]Karyopharm Therapeutics, Natick, MA, USA

[7]National University Cancer Institute, National University Hospital Singapore, Singapore

Abstract

Esophageal squamous cell carcinoma (ESCC) is a world-wide prevalent cancer, which is particularly common in certain regions of Asia. Here we report the whole-exome or targeted deep sequencing of 139 paired ESCC cases, and analysis of somatic copy number variations (SCNV) of over 180 ESCCs. We identified novel significantly mutated genes such as *FAT1*, *FAT2*, *ZNF750*

[9]Correspondence should be addressed to M-R.W. (wangmr2015@126.com) or D-C.L. (dchlin11@gmail.com).
[8]These authors contributed equally to this work.

URLs: dbSNP, http://www.ncbi.nlm.nih.gov/projects/SNP/; 1000 Genomes Project, http://www.1000genomes.org/; CNAG/AsCNAR, http://www.genome.umin.jp/; MutSigCV, http://www.broadinstitute.org/cancer/cga/mutsig; TCGA, http://cancergenome.nih.gov/; COSMIC, http://cancer.sanger.ac.uk/cancergenome/projects/cosmic/; Clinical trials database, http://clinicaltrials.gov/;CCLE, http://www.broadinstitute.org/ccle/home; TumorScape, http://www.broadinstitute.org/tumorscape/pages/portalHome.jsf; IGV, http://www.broadinstitute.org/igv; UniProt, http://www.uniprot.org/; Box Plot, http://en.wikipedia.org/wiki/Box_plot; BRB-CGH tools, http://linus.nci.nih.gov/BRB-ArrayTools.html; MD-SeeGH,www.flintbox.ca. Sequence Read Archive, http://www.ncbi.nlm.nih.gov/sra.

Accession code. Deep sequencing files have been deposited into Sequence Read Archive under accession number SRP033394.

Author Contributions: D-C.L., M-R.W. and H.P.K. designed the study and wrote the manuscript. D-C.L., J-J.H., Y.N.,Y.S., Y.O., X.M., L.X., A.M.V., L-W.D. and M.G. performed experiments. D.Y, J-J.H., Z-Z.S., L.S., Y-Y.J., W-Y.G., T.G., Y.Z. and X.X. coordinated sample collection and processing. O.K. and S.S. provided KPT-330 and structurally analyzed XPO1 point mutation. D-C.L., J-J.H., Y.N., S.O., M-R.W. and H.P.K. analyzed and discussed the data. Y.N., H.Y., L-Z.L., Y.S., and Y.O. performed bioinformatical analysis.

Competing Financial Interests: O.K. and S.S. are employees of Karyopharm Therapeutics Incorporated. The remaining authors declare no conflict of interest.

and *KMT2D*, in addition to previously discovered ones (*TP53*, *PIK3CA* and *NOTCH1*). Further SCNV evaluation, immunohistochemistry and biological analysis suggested their functional relevance in ESCC. Notably, RTK-MAPK-PI3K pathways, cell cycle and epigenetic regulation are frequently dysregulated by multiple molecular mechanisms in this cancer. Moreover, our approaches uncovered many novel druggable candidates, and XPO1 was further explored as a therapeutic target because of its mutation and protein overexpression. Together, our integrated study unmasks a number of novel genetic lesions in ESCC and provides an important molecular foundation for understanding esophageal tumors and developing therapeutic targets.

ESCC is one of the most common malignant diseases in the world and especially in China, where it is the fourth most common cause of cancer-related deaths[1]. Unlike cancers that have been extensively studied, such as breast and colon cancers, the outcome of ESCC remains unchanged during the last several decades, with a five-year survival rate ranging from 15% to 25%[2]. We and others have revealed frequent somatic copy number variations (SCNV) involving 3q26[3], 9p21[4], 11q13.3[5] and 8q24.3[6], as well as somatic mutations in *PIK3CA*[7], *TP53*[8]and *NOTCH1*[8] in ESCC. However, in general, understanding of the genomic abnormalities in this disease is limited to studies of small size of cohorts[4,6,7,9-12], including a recent whole-exome sequencing approach of 12 ESCCs[8]. Thus, a compelling need exists to extensively identify genomic abnormalities underlying ESCC, for elucidating its molecular basis and guiding the development of effective targeted therapies.

We firstly sequenced whole exomes (WES) of 20 paired ESCC germline/tumors (Discovery Cohort, mean coverage 79×, Supplementary Tables 1a, 2a). Transcriptome sequencing (RNA-seq) was also performed on 4 of these 20 tumors. A total of 1,186 non-silent somatic mutations (affecting 1,042 genes) were identified (Supplementary Table 3), a mutation rate comparable to those of most adult solid tumors[13] (Supplementary Fig. 1). We extensively validated 362 candidate somatic mutations with Sanger sequencing (True positive rate = 93.1%, Supplementary Table 3). Intratumoral clonality analysis showed that both biclonal and multiclonal signatures existed in ESCC (Supplementary Fig. 2). Cross comparing the WES with RNA-seq data from the same tumors revealed that 61% of the mutated genes were transcribed (Supplementary Table 4), which is comparable to the value reported on breast cancer[14].

To evaluate the prevalence of these mutated genes from Discovery Cohort, we sequenced all of their coding exons with 119 additional matched ESCC germline/tumors, as well as 10 ESCC cell lines (Frequency Cohort, mean coverage 111×, Supplementary Tables 1b, 2b). To cover more comprehensively the mutational events in this disease, we also included an additional 277 genes which were discovered in the previous WES study of 12 ESCCs[8] and/or were causally implicated in other human cancers (Cancer Gene Census; see URLs; Supplementary Table 5). As a result, a total of 1,847 non-silent somatic mutations were identified with an average of 15 mutations per case (True positive rate = 96.2%, Fig. 1a; Supplementary Table 6). Remarkably, mutational spectrums revealed from Discovery and Frequency Cohort are almost identical (Supplementary Fig. 3a), suggesting that our targeted sequencing approach comprehensively unmasked most of the mutational events in DNA coding regions in ESCC. Of note, trinucleotide signature analysis suggested that DNA

cytidine deaminase APOBEC3B is responsible for ESCC mutagenesis[15-17] (Fig. 1b, Supplementary Fig.3b), and indeed, APOBEC3B expression was clearly up-regulated in ESCC tumors (Fig. 1c). We observed that 609 genes were mutated in 2 or more samples, with 62 genes mutated at a frequency over 5% (Supplementary Fig. 3c). To identify mutations conferring selective growth advantages ("Driver Mutations"), we applied the algorithm MutSigCV[13], which corrects for variation by incorporating patient-specific mutational spectrum, gene-specific background mutational burden and also by measuring gene expression level and replication time. As a result, we calculated that 13genes were significantly mutated (False discovery rate $q < 0.2$). Importantly, many of these significantly mutated genes had not previously been implicated in ESCC.

To interrogate SCNV in ESCC, we examined 22 tumors with SNP-array (18 from Discovery Cohort), as well as 59 samples with array-CGH[18]. We further comprehensively analyzed three additional SNP-array datasets measuring primary ESCCs[4,11,12] (Supplementary Table 7), resulting in a total of 184 analyzable primary ESCC samples. We focused on focal SCNV, defined as narrow regions (typically <100 kb) exhibiting high-amplitude of copy number changes (Online Methods), which has more probability to contain cancer genes. This approach identified 14 recurrent focal SCNVs, with the most frequent amplification peak spanning the *CCND1* gene on 11q13.2 (Supplementary Table 7). Additional peaks involving important cancer genes such as *EGFR, MYC, KRAS* and *CDKN2A*were found. Notably, *FGFR1* was shown to be frequently amplified, which has not been reported before in ESCC. To confirm this observation, we examined an additional 53 ESCC tumors with fluorescence in situ hybridization (FISH) and found that *FGFR1* was amplified in 11 samples (Fig. 2a; Supplementary Table 7). Furthermore, with immunohistochemistry (IHC), we found that the FGFR1 protein was up-regulated in 17.3% ESCC tumors (Fig. 2b; Supplementary Table 8a). Given that *FGFR* amplification predicts for sensitivity to targeted inhibitors in several other solid tumors[19], our results suggest that FGFR1 is a potential therapeutic target in ESCC.

We next sought to understand dysregulated pathways in ESCC. As we previously reported protein alterations in ESCC using meta-analysis[20], here we also took into account protein overexpression evidence. Mitogen-activated protein kinase (MAPK) (Fig. 2d, $P = 0.0005$, Supplementary Table 9a, Online Methods) and phosphatidylinositol 3-kinase (PI3K)pathways ($P = 0.0004$) are augmented by multiple mechanisms: i) amplification and overexpression of RTKs, KRAS and PIK3CA; ii) activation mutations of *ERBB4* and *PIK3CA*; iii) inactivation mutations of *PTEN*, *MAP3K13* and *MAP3K15*. In addition, *IL7R* amplification and *JAK1* mutations were identified, which will likely activate JAK-STAT3 signaling (P=0.0006). Supportively, we have shown that p-STAT3 was elevated in ESCC[21], which transforms esophageal epithelial cells cooperatively with amplified *SOX2*[22]. Cell cycle progression (Fig. 2e, $P = 1.63E-05$) is altered mostly by *CCND1* amplification, *CDKN2A* deletion/mutation and *TP53* mutation. As a negative regulator of c-Myc, frequent *FBXW7* mutations were observed in our investigation (Fig. 2c), confirming a recent report of this gene in ESCC[8]. Importantly, we next examined FBXW7 protein expression with IHC and found its mutation led to loss of the protein (Fig. 2c). Moreover, in an additional cohort ($n = 40$), we determined that FBXW7 protein was down-regulated in 33% tumors

(Supplementary Fig.7; Supplementary Table 8b), further demonstrating its relevance in ESCC. Another prominent enrichment of mutated genes in ESCC are those implicated in epigenetic modifications (P = 0.0013, Fig. 2f, Supplementary Table 9b), such as members of SWI/SNF complex (*ARID2* and *PBRM1*), histone methyltransferases *KMT2D* and *KMT2C*, and demethylase *KDM6A*.

ZNF750 is a poorly studied nuclear protein that is up-regulated in differentiated skin keratinocytes[23,24]. We observed that *ZNF750* was significantly mutated in ESCC (q = 1.24E-06, Fig. 3a). Strikingly, analysis of public datasets revealed that *ZNF750* is largely mutated in squamous cell carcinomas, with most of them presenting truncating mutations (Supplementary Fig. 4b). Supportively, ESCC harbors a much higher mutational burden affecting *ZNF750* than esophageal adenocarcinoma. The similar pattern was also observed when comparing lung SCC to lung adenocarcinoma. From Cancer Cell Line Encyclopedia (CCLE, see URL) results, we found that ZNF750 mRNA was expressed at a much higher level in ESCC and UASCC than any other non-squamous cancer cell lines (Supplementary Fig. 4a). These data suggest that *ZNF750* somatic mutations are biologically relevant in squamous cell malignancy. In addition, we identified that *ZNF750* was focally deleted in 3.4% ESCC tumors (Fig. 3b) and ZNF750 mRNA level was significantly under-expressed in esophageal tumors compared with normal tissue (Fig. 3c). Moreover, our IHC approach showed that in normal esophageal epithelial, ZNF750 protein displayed strong nuclear staining in the suprabasal layer of cells and above; whereas in ESCC tumors, ZNF750 was expressed at much lower levels (Fig. 3d; Supplementary Table 8c). Importantly, in ESCC cells with wildtype endogenous ZNF750 expression, depletion of ZNF750 promoted cell proliferation (Fig. 3e), associated with a decreased expression of the genes implicated in late epithelial differentiation, whereas ectopic expression of ZNF750 led to the up-regulation of these genes (Supplementary Fig. 4c). Moreover, 12-O-tetra-decanoylphorbol-13-acetate (TPA), a well-characterized differentiation-induction agent which has also been commonly used to promote ESCC differentiation[25,26], markedly enhanced ZNF750 expression (Fig. 3f), with a concomitant inhibition of cell proliferation (Supplementary Fig. 4d). Notably, ectopic expression of ZNF750 further promoted the TPA-induced growth-suppression (Fig. 3g). Collectively, these results indicate that ZNF750 might function as a novel tumor suppressor in ESCC through regulating squamous cell differentiation.

FAT family is comprised of FAT1, FAT2, FAT3 and FAT4, which are cadherin superfamily members homologous to *Drosophila* gene *fat*. Very recently, *FAT1*has been reported as a tumor suppressor in glioblastoma, colorectal cancer and HNSCC[27]. However, the precise role of *FAT* genes in cancer still remains inconclusive and needs further characterization[28,29]. Our data revealed that ESCC harbored very frequent, mutually-exclusive truncating mutations affecting *FAT1*, *FAT2* and *FAT3* compared to other solid tumors (Figs. 4a-b, Supplementary Fig. 5a). Among *FAT1*-mutated tumors, two samples were also analyzed with SNP-array, and we discovered loss of heterozygosity of the *FAT1* gene in both tumors (Supplementary Fig.5b), supporting Knudson's two-hit model. We next found that homozygous deletions of*FAT1* occurred in 3.4% ESCCs (Fig. 4c). Furthermore, IHC staining demonstrated that FAT1 protein expression was down-regulated in ESCC (Fig. 4d). To study the function of *FAT* gene inactivation in ESCC, we first silenced wildtype

FAT1 expression with siRNA, and observed increase in cell proliferation (Fig. 4e). On the other hand, ectopic expression of FAT1 cDNA[27] significantly inhibited both cell proliferation and colony formation in soft agar (Supplementary Fig. 6). Importantly, depletion of FAT2 with shRNA promoted ESCC growth in vivo (Figs. 4f-g). Together, these genetic/expression alterations and biological evidence strongly suggest that *FAT1* and *FAT2* likely encode tumor suppressors which are frequently disrupted in ESCC.

In mammalian cells, the chief mediator of protein nuclear export is exportin 1 (XPO1).Due to its ability to export a number of tumor suppressors, targeting XPO1 has been considered as an anti-neoplastic approach[30]. We found one missense mutation D624G affecting *XPO1*. Importantly, this mutation is identical to the one discovered in chronic lymphocytic leukemia[31]. Structural modeling analysis revealed that Asp624 is part of the binding sites of its conventional cargo, such as Snurportin[32,33], forming a salt bridge with Snurportin's Lys144 (Fig. 5a). D624G mutation presumably reduces the affinity of interactions due to loss of the salt bridge. This alteration may accelerate the turnover of XPO1 from “bound” to “unbound” state and enhance its exporting efficiency. We next analyzed the expression levels of XPO1's mRNA and protein and found that they were frequently overexpressed in ESCC tumor samples (Figs. 5b-c). Moreover, XPO1 overexpression positively correlated with larger tumor size ($P = 0.016$, Supplementary Table 8d). Notably, the *XPO1*-mutated tumor also showed up-regulated protein level compared with the matched adjacent normal esophageal epithelium, indicating a gain-of-function phenotype (Fig. 5b). We next silenced XPO1 gene expression with shRNA, and noticed the induction of apoptosis (as evidenced by cleaved-PARP) and retardation of cell proliferation (Figs. 5d, e).To explore whether XPO1 is druggable in ESCC, we treated ESCC cells with a novel oral, small-molecule inhibitor, KPT-330, which specifically blocks its function by binding to the active site Cys528[34-36]. Submicromolar concentrations of KPT-330 inhibited ESCC cell proliferation and induced significant apoptosis (Figs. 5f, g). Inhibition of XPO1 with either shRNA or KPT-330 altered the expression of its known cargos (such as P53), as well as indirect targets including Cyclin D1, c-Myc, PUMA and BIM, which might be due to various novel mechanisms that we and others have recently identified[37-43] (Figs. 5e, h). Given that frequent overexpression of XPO1 protein is clinically relevant[44-47] and functionally contributes to the cellular malignant phenotype, targeting XPO1 in those patients with XPO1 up-regulation might offer potential benefits in ESCC.

In an effort to identify comprehensively therapeutic targets in ESCC, we correlated genomic mutations, amplifications, and mRNA/protein up-regulations[48-51] in both primary tumors and cancer cell lines, with novel targeted therapeutic approaches. We chose those targeting approaches that have been approved for clinical use[52,53] or are under evaluation in clinical trials (see URL). As a result, we identified 31 genes with potentially actionable alterations in ESCC. Recurrent candidate druggable targets included ERBB, HDAC and PI3K family, XPO1, FGFR1, TP53, JAK-STAT3 and MTOR-RPS6K signaling (Supplementary Table 10). Importantly, most of the targets and pathways discovered here have not previously been considered as actionable targets in ESCC. These results suggest that many novel potential therapeutic targets exist in ESCC that need further investigation.

In summary, we report the mutational landscape of 139 ESCCs as well as SCNV overview of 184 ESCC cases. A number of novel mutated/altered genes and pathways were identified with statistical and biological evidence of growth selection, indicating that they likely contribute to esophageal tumorigenesis. Together with XPO1, our analysis proposes many potential therapeutic targets, which offer opportunities to address a typically chemo-resistant cancer.

Online Methods

Sample collection and histopathological assessment

ESCC tissue samples were collected from Cancer Institute/Hospital, Chinese Academy of Medical Sciences (CAMS) and Linxian Cancer Hospital. All the samples used in this study were residual specimens collected after diagnosis. No patient received treatment before sample collection. Matched normal tissues (germline controls) were collected from adjacent esophageal epithelial five centimeters away from the border of surgical area. All tumor/normal samples were subject to hematoxylin staining and histopathological review to assess the presence of tumor cells, normal esophageal epithelial cells, lymphocytic infiltration and necrotic cells. Tumor cellularity was scored visually in a semi-quantitative fashion and only those with >70% malignant cells were chosen for DNA/RNA sequencing. All patients signed independent informed consent forms for the sampling and molecular analyses. This study has been approved by the Ethics Committee/IRB of Cancer Institute/Hospital, CAMS and Linxian Cancer Hospital.

Cell culture and related chemicals

All of the human ESCC cell lines and 293T were grown in Dulbecco modified Eagle medium (DMEM) with 10% fetal calf serum (FCS) and were maintained at 37°C in a 5% CO2 air humidified incubator. ESCC cell lines KYSE30, KYSE50, KYSE70, KYSE110, KYSE150, KYSE450, KYSE510 and YES2 were kindly shared by Yutaka Shimada (Faculty of medicine, Kyoto University). KYSE140 and KYSE180 were generously provided by Dr. Xin-Yuan Guan. All ESCC cell lines were regularly authenticated and tested for absence of mycoplasma recently[55]. TPA was purchased from Sigma-Aldrich. KPT-330 was provided by Karyopharm Therapeutics.

Short-term cell proliferation assays

Cells were placed into 96-well plates at 2-4 × 10^3 cells/well and incubated for an additional 4-5 days in DMEM with 1% - 10% FCS. The MTT (3-(4, 5-dimethylthiazol–2-yl) -2, 5-diphenyl tetrazolium bromide) assay was performed as described previously[56].

Assessment of apoptosis

Annexin V assay (BD Pharmingen) was performed to assess apoptosis according to the manufacturer's instructions. Briefly, cells were harvested after exposure to KPT-330, washed twice with PBS, incubated with FITC/PE-conjugated Annexin V and propidium iodide/7-AAD for 15 min, and measured by flow cytometry (FCM) using FACScan (Becton Dickinson).

Xenografts in NOD/SCID mice

Gender-matched NOD/SCID mice were provided by Cancer Science Institute of Singapore at 5-6 weeks of age. 2×10^6 of KYSE150 cells (Scramble and shFAT2 stable cells) were mixed with 100 μl of Matrigel solution (BD Biosciences) per injection; and the mixture was injected subcutaneously on the upper flanks of NOD/SCID mice. Mice were randomly allocated to either Scramble or shFAT2 groups. After 19 days, the mice were sacrificed to weigh and analyze the dissected tumors. No blinding of investigators was performed. No statistical methods were used to determine the sample size of mice. Animal study was done in compliance with ethical regulations of relevant Institutional Animal Care and Use Committee.

Reverse transcription and Real-time PCR

Total RNA was reverse transcribed to cDNA with Superscript III (Invitrogen) according to manufacturer's protocols. Real-time PCR reactions were performed in triplicates for every sample in 7500 Real-time PCR System (Applied Biosystems). Primers are listed in Supplementary Table 13a.

Lentiviral based expression and shRNA vectors

The open reading frame (ORF) of human *FAT1 and ZNF750* transcripts were generously provided by Timothy Chan's group from Memorial Sloan-Kettering Cancer Center[27] and Paul Khavari's group from Veterans Affairs Palo Alto Healthcare System[24], respectively. Both ORFs were sub-cloned into lentiviral based expression vector SHC003 (Sigma-Aldrich) using *Nhe* I and *Fse* I cloning sites. SHC003-Turbo-GFP was used as control (Sigma-Aldrich). The lentiviral based shRNA vectors (shXPO1 and shFAT2 sequences are listed in Supplementary Table 13b) were generated with PLKO.1 backbone (Sigma-Aldrich) using *Age* I and *EcoR* I cloning sites. SHC002-Scramble shRNA was used as control (Sigma-Aldrich). The cloning primers are listed in Supplementary Table 13c.

Transfections, viral particle production and infection

ESCC cells and 293T cells were transfected with Lipofectamine 2000 according to the manufacturer's instructions (Invitrogen). siRNA sequences targeting *FAT1* or *ZNF750* are listed in Supplementary Table 13d. Lentiviral particles were produced and harvested using MISSION Lentiviral Packaging System (Sigma-Aldrich). The ESCC cells were infected with the lentiviral particles for 48 hours in the presence of 8 ug/ml polybrene (Sigma-Aldrich).

Whole exome sequencing (WES) and targeted deep sequencing (TDS)

1.5 μg (WES)or 1 μg (TDS) of genomic DNA was sonicated to generate a peak target size of 200 bp. DNA was captured using the SureSelect® Human All Exon 50M (WES) or customized cRNA beads (Supplementary Table 14, TDS) according to the manufacturers' protocols. Captured DNAs were subjected to massively parallel sequencing using HiSeq2000 with 75-100 bp paired-end reads.

To detect somatic nucleotide variations from WES, the previously described in-house algorithms were used[57-59]. Briefly, the sequencing reads were aligned to a human reference genome (hg19) using BWA version 0.5.8 with default parameters. PCR duplicate reads were removed using Picard (http://www.picard.sourceforge.net/). Before summarizing base call data, low quality reads were eliminated, including those reads which have either more than 5 mismatches to the reference sequences or whose mapping quality was less than 30. The significance of each candidate mutation was evaluated by Fisher's exact test by enumerating the number of the reference base and the candidate SNV in both tumor and germline control. Candidate mutations with p-values less than 0.01 were adopted as provisional candidates for somatic mutations. In addition, the following nucleotide positions were eliminated from further analysis, including those positions at which the depth is less than 10 in either tumor or control, or the most frequent SNV or indel accounts for less than 7% of all reads in the tumor. Germline SNPs were eliminated using sequencing data from paired normal DNA. Finally, a list of candidate somatic mutations was generated by excluding synonymous SNVs and other variants registered in dbSNP131, 1,000 genomes, or our in-house SNP database constructed from 180 patients[57,58].

To make a more rigorous somatic mutation calling with the TDS approach of Frequency Cohort, the following nucleotide positions were further removed: the supporting depth from both directions was less than 5 in either tumor or control, or the most frequent SNV or indel accounts for less than 8% of all reads in the tumor.

To detect probable somatic mutations of ESCC cell lines which do not have paired germline controls, the following nucleotide positions were further removed: the supporting depth from both directions is less than 5, or the most frequent SNV or indel accounts for less than 8% of all reads, or the frequency of the SNV or indel is between 45% and 55% without copy number abnormalities.

Tissue microarray (TMAs) and immunohistochemistry (IHC)

Paraffin-embedded tissue microarrays (TMAs) containing 50 primary ESCC tumors and the corresponding normal epithelia were used for IHC. For each case, histologically normal tissues adjacent to tumors were examined as control. TMA slides were initially deparaffinized using xylene, rehydrated with xylene and ethanol, immersed in 3% hydrogen peroxide solution for 10 min, heated with citrate at 95°C for 25 min, and cooled at room temperature for 60 min. The slides were incubated overnight at 4°C with the following antibodies: XPO1 (sc-5595, Santa Cruz Biotechnology; 1:50), ZNF750 (HPA023012, Sigma-Aldrich Inc.; 1:100), FAT1 (HPA023882, Sigma-Aldrich Inc.; 1:25), or FBXW7 (H00055294-M02, Abnova; 1:200), FGFR1 (9740, Cell Signaling Technology, 1:25) and visualized using PV-9000 Polymer Detection System following the manufacturer's instructions (Golden Bridge International, USA). Counterstaining was carried out with hematoxylin. The results were separately evaluated by two pathologists. Protein expression was evaluated on the basis of staining intensity, graded on the following scale: 0 (negative), 1 (weak), 2 (moderate), and 3 (strong).

Western blotting (WB)

Cells were lysed on ice with lysis buffer (50 mM Tris-HCl, pH 7.4, 150 mMNaCl, 0.5% Nonidet P-40) containing complete protease and phosphatase inhibitor cocktail (Roche). The rest procedures for WB was performed as described previously[60]. Antibodies specific for cyclin B1 (4135), cleaved-PARP (9541), $p21^{WAF1}$(2947) and BIM (2933) were purchased from Cell Signaling Technology. Antibodies specific for c-Myc (SC-788), cyclin D1 (sc-8396), Bcl-xl (sc-8392), P53 (sc-6243), XPO1 (sc-5595) and PUMA (sc-28226) were purchased from Santa Cruz Biotechnology. Antibody against FAT1 (HPA023882), ZNF750 (HPA023012) and β-Actin (A5316) were purchased from Sigma-Aldrich.

RNA extraction and paired-end sequencing

6 μg of total RNA from each sample was extracted according to the manufacturer's instruction of RNeasy Micro kit (QIAGEN, Germany), followed by mRNA purification using Oligotex mRNA Mini Kit (QIAGEN, Germany). RNA quality was assessed by Agilent 2100 Bioanalyzer, and the RNA integrity number was > 7.0, with 28S/18S > 0.7. The cDNA libraries were constructed following the TruSeq RNA Sample Preparation Guide (Illumina, USA). Briefly, first-strand and second-strand cDNAs were synthesized from the purified mRNAs, and fragmented by ultrasonic waves. After performing end repair, cDNAs were modified by 3′-end adenylation and adaptor ligation. PCR was performed to enrich the cDNA templates in order to complete the cDNA library construction. The concentration of the final cDNA library was more than 1 ng/μl, and the size of the cDNA fragments was 350-400 bp. Sequencing reagents were prepared according to the Genome Analyzer IIx User Guide (Illumina). cDNA fragments were treated with cluster generation and loaded to the lanes of Illumina flow cells, and paired-end sequencing was performed using the 2×100 nt multiplex program. The raw sequenced reads yielded more than 50 million bases per sample.

Array-based CGH and SNP-array

Array-CGH experiments were performed using standard protocols as previously described (44K human genome CGH microarrays, Agilent Technologies, Santa Clara, CA)[9]. Human genomic DNA (PROMEGA, Warrington, UK) was used as reference. Briefly, 500 ng of reference genomic DNA and tumor DNA were digested with *Alu I* and *Rsa I* (PROMEGA, Warrington, UK). The resulting reference DNA was labeled with cyanine-5 dUTP and the tumor DNA with cyanine-3 dUTP, respectively (Agilent Technologies, Santa Clara, CA). After clean-up, labeled DNA probes were mixed and hybridized to CGH microarray for 24h-40h. Washing, scanning and data extraction were performed according to standard protocols. Array CGH data were analyzed using Genomic Workbench (Agilent), BRB-CGH tools and MD-SeeGH (See URL). Mean $\log_2$ tumor/reference ratio of all probes in a chromosome region > 1.0 was determined as high-amplitude amplification, and < -1.0 as high-amplitude deletion. These values were converted based on the following presumptions: (i) for amplifications, copy number > 6 was present in more than 70% cancer cell populations; (ii) for deletions, loss of both alleles was present in more than 70% cancer cell populations, and (iii) normal cell contamination was less than 30%[60].

Human 250K arrays (Affymetrix) were used for SNP-array assays, and results were analyzed as previously described using CNAG/AsCNAR software[61,62].

Interphase cell nuclei preparations and fluorescence in situ hybridization (FISH)

In order to examine interphase cell nuclei, ESCC tissue samples were cut into small pieces in phosphate-buffered saline (PBS), followed by treatment with a hypotonic solution (0.075 mol/L KCl) for 30 minutes and three successive changes of the fixative solution (methanol/acetic acid, 3:1). Interphase cell nuclei in suspension were kept at 4°C overnight and then stored at -20°C. Prior to the hybridization, the nuclear suspensions were dropped onto slides and dried at room temperature for 2-3 days.

FISH was performed on the interphase cell nuclei. By random priming using BioPrime DNA labeling system (Invitrogen), chromosome enumeration probes (CEP) and bacterial artificial chromosome (BAC)-DNA probes were directly labeled with Green-dUTP (Abbott Molecular, USA) and Cy3-dUTP (GE Healthcare, USA), respectively. BAC-DNA clones selected for *FGFR1* were NONSC11F1 (Chr8: 38,170,901-38,368,835).

The slides for FISH analyses were pretreated with RNase A (100 mg/ml in 2 × saline sodium citrate [SSC]) and pepsin (50 mg/ml in 0.01 mol/l HCl), subsequently denatured in 70% formamide/2 × SSC at 73°C-75°C for 3 minutes, quickly cooled with two rinses of 2 × SSC at 4°C, dehydrated in a gradient series of ethanol (75%, 85% and 100%), and air dried. The labeled probes were precipitated, and re-dissolved in the hybridization solution (50% formamide, 10% dextran sulfate, 1% Tween-20, 2 × SSC), denatured at 75°C for 8 minutes, and quick-chilled on ice for 2 minutes. Hybridization was performed in a humid chamber at 37°C for 24-48 hours. Post-hybridization washes were performed in 50% formamide/2 × SSC for 15 minutes at 43°C and were performed twice for 3 minutes each in 2 × SSC. The slides were dehydrated in 75%, 85% and 100% ethanol, air dried, counterstained with 40,6-diamidino-2-phenylindole (DAPI) (1 mg/ml) and covered with coverslips.

Microscopy and digital image analysis

FISH images were captured using a Zeiss Axio fluorescence microscope equipped with a cooled charged-coupled device (CCD) camera (Princeton Instruments, USA) or a JAI M4 Plus CCD camera (Metasystems International, Germany). All of the fluorescent images were captured with individual single-band-pass filters specific for visualizing DAPI, Green, Cy3 fluorochromes. Pseudo-color images were constructed and analyzed using MetaMorph (Universal Imaging Corporation, USA) or Metacyte module of Metafer imaging systems (Metasystems International).

Amplifications were assessed as the difference value between BAC-DNA and CEP probes was at least 2 in more than 30% cells. Cluster signals and ratios (BAC-DNA/CEP) > 2 were judged as the high-level amplifications.

Analysis of significantly altered pathways

To analyze significantly altered pathways, we performed unbiased Gene Ontology (GO) enrichment in the overall ranked MutSigCV list[63]. As parallel approaches, WEB-based Gene SeT AnaLysis Toolkit (WebGestalt) was applied to identify the KEGG pathways that are enriched in the MutSigCV list. Multiple-test corrected P-values were calculated using

hypergeometric test for pathways that are enriched compared to human genome reference gene set[64,65].

Statistical analysis

Q value for significantly mutated genes were calculated using default setting according to MutSigCV[13]. The *p* value of the two mutational events as mutually exclusive events is defined by calculating the joint probability. The statistical analyses of the following assays were conducted using the two tailed Student's t-test upon verification of the assumptions (e.g., normality), otherwise the non-parametric test was applied: short-term cell proliferation, xenografts proliferation, q-PCR, apoptosis induction, mRNA levels examined from GSE20347[11], GSE23400[54] and CCLE.

Supplementary Material

Refer to Web version on PubMed Central for supplementary material.

Acknowledgments

We thank Patrick Tan and Zhijiang Zang for generously sharing related facilities. We also thank Blanche and Steve Koegler for their generous support. This work is supported by National High-Tech R&D Program of China 2012AA02A503 and 2012AA02A209 (M-R.W.), National Natural Science Foundation of China 81330052(M-R.W.), NIH grant R01CA026038-35 (H.P.K.), National Research Foundation Singapore and the Singapore Ministry of Education under the Research Centers of Excellence initiative (H.P.K), and Singapore Ministry of Health's National Medical Research Council under its Singapore Translational Research (STaR) Investigator Award to H.P.K.

References

1. Zhao P, Dai M, Chen W, Li N. Cancer trends in China. Jpn J Clin Oncol. 2010; 40:281–5. [PubMed: 20085904]
2. Pennathur A, Gibson MK, Jobe BA, Luketich JD. Oesophageal carcinoma. Lancet. 2013; 381:400–12. [PubMed: 23374478]
3. Yang YL, et al. Amplification of PRKCI, located in 3q26, is associated with lymph node metastasis in esophageal squamous cell carcinoma. Genes Chromosomes Cancer. 2008; 47:127–36. [PubMed: 17990328]
4. Bass AJ, et al. SOX2 is an amplified lineage-survival oncogene in lung and esophageal squamous cell carcinomas. Nat Genet. 2009; 41:1238–42. [PubMed: 19801978]
5. Luo ML, et al. Amplification and overexpression of CTTN (EMS1) contribute to the metastasis of esophageal squamous cell carcinoma by promoting cell migration and anoikis resistance. Cancer Res. 2006; 66:11690–9. [PubMed: 17178864]
6. Hu N, et al. Genomic characterization of esophageal squamous cell carcinoma from a high-risk population in China. Cancer Res. 2009; 69:5908–17. [PubMed: 19584285]
7. Shigaki H, et al. PIK3CA mutation is associated with a favorable prognosis among patients with curatively resected esophageal squamous cell carcinoma. Clin Cancer Res. 2013; 19:2451–9. [PubMed: 23532889]
8. Agrawal N, et al. Comparative genomic analysis of esophageal adenocarcinoma and squamous cell carcinoma. Cancer Discov. 2012; 2:899–905. [PubMed: 22877736]
9. Shi ZZ, et al. Genomic alterations with impact on survival in esophageal squamous cell carcinoma identified by array comparative genomic hybridization. Genes Chromosomes Cancer. 2011; 50:518–26. [PubMed: 21484929]

10. Hirasaki S, et al. BAC clones related to prognosis in patients with esophageal squamous carcinoma: an array comparative genomic hybridization study. Oncologist. 2007; 12:406–17. [PubMed: 17470683]
11. Hu N, et al. Genome wide analysis of DNA copy number neutral loss of heterozygosity (CNNLOH) and its relation to gene expression in esophageal squamous cell carcinoma. BMC Genomics. 2010; 11:576. [PubMed: 20955586]
12. Beroukhim R, et al. The landscape of somatic copy-number alteration across human cancers. Nature. 2010; 463:899–905. [PubMed: 20164920]
13. Lawrence MS, et al. Mutational heterogeneity in cancer and the search for new cancer-associated genes. Nature. 2013
14. Shah SP, et al. The clonal and mutational evolution spectrum of primary triple-negative breast cancers. Nature. 2012; 486:395–9. [PubMed: 22495314]
15. Burns MB, Temiz NA, Harris RS. Evidence for APOBEC3B mutagenesis in multiple human cancers. Nat Genet. 2013
16. Burns MB, et al. APOBEC3B is an enzymatic source of mutation in breast cancer. Nature. 2013; 494:366–70. [PubMed: 23389445]
17. Roberts SA, et al. An APOBEC cytidine deaminase mutagenesis pattern is widespread in human cancers. Nat Genet. 2013
18. Shi ZZ, et al. Consistent and differential genetic aberrations between esophageal dysplasia and squamous cell carcinoma detected by array comparative genomic hybridization. Clin Cancer Res. 2013; 19:5867–78. [PubMed: 24009147]
19. Guagnano V, et al. FGFR genetic alterations predict for sensitivity to NVP-BGJ398, a selective pan-FGFR inhibitor. Cancer Discov. 2012; 2:1118–33. [PubMed: 23002168]
20. Lin DC, Du XL, Wang MR. Protein alterations in ESCC and clinical implications: a review. Dis Esophagus. 2009; 22:9–20. [PubMed: 18564170]
21. Zhang Y, et al. Reciprocal activation between PLK1 and Stat3 contributes to survival and proliferation of esophageal cancer cells. Gastroenterology. 2012; 142:521–530 e3. [PubMed: 22108192]
22. Liu K, et al. Sox2 cooperates with inflammation-mediated Stat3 activation in the malignant transformation of foregut basal progenitor cells. Cell Stem Cell. 2013; 12:304–15. [PubMed: 23472872]
23. Cohen I, et al. ZNF750 is expressed in differentiated keratinocytes and regulates epidermal late differentiation genes. PLoS One. 2012; 7:e42628. [PubMed: 22936986]
24. Sen GL, et al. ZNF750 is a p63 target gene that induces KLF4 to drive terminal epidermal differentiation. Dev Cell. 2012; 22:669–77. [PubMed: 22364861]
25. Yu X, et al. Differentiation-associated genes regulated by TPA-induced c-Jun expression via a PKC/JNK pathway in KYSE450 cells. Biochem Biophys Res Commun. 2006; 342:286–92. [PubMed: 16480952]
26. Chen H, et al. S100A14 is a novel modulator of terminal differentiation of esophageal squamous cell carcinoma. Mol Cancer Res. 201310.1158/1541-7786
27. Morris LG, et al. Recurrent somatic mutation of FAT1 in multiple human cancers leads to aberrant Wnt activation. Nat Genet. 2013; 45:253–61. [PubMed: 23354438]
28. Dikshit B, et al. FAT1 acts as an upstream regulator of oncogenic and inflammatory pathways, via PDCD4, in glioma cells. Oncogene. 2012; 32:3798–808. [PubMed: 22986533]
29. de Bock CE, et al. The Fat1 cadherin is overexpressed and an independent prognostic factor for survival in paired diagnosis-relapse samples of precursor B-cell acute lymphoblastic leukemia. Leukemia. 2012; 26:918–26. [PubMed: 22116550]
30. Turner JG, Dawson J, Sullivan DM. Nuclear export of proteins and drug resistance in cancer. Biochem Pharmacol. 2012; 83:1021–32. [PubMed: 22209898]
31. Landau DA, et al. Evolution and impact of subclonal mutations in chronic lymphocytic leukemia. Cell. 2013; 152:714–26. [PubMed: 23415222]
32. Paraskeva E, et al. CRM1-mediated recycling of snurportin 1 to the cytoplasm. J Cell Biol. 1999; 145:255–64. [PubMed: 10209022]

33. Monecke T, et al. Crystal structure of the nuclear export receptor CRM1 in complex with Snurportin1 and RanGTP. Science. 2009; 324:1087–91. [PubMed: 19389996]
34. Ranganathan P, et al. Preclinical activity of a novel CRM1 inhibitor in acute myeloid leukemia. Blood. 2012; 120:1765–73. [PubMed: 22677130]
35. Etchin J, et al. KPT-330 inhibitor of CRM1 (XPO1)-mediated nuclear export has selective anti-leukaemic activity in preclinical models of T-cell acute lymphoblastic leukaemia and acute myeloid leukaemia. Br J Haematol. 2013; 161:117–27. [PubMed: 23373539]
36. Etchin J, et al. Antileukemic activity of nuclear export inhibitors that spare normal hematopoietic cells. Leukemia. 2013; 27:66–74. [PubMed: 22847027]
37. Chen L, Fischle W, Verdin E, Greene WC. Duration of nuclear NF-kappaB action regulated by reversible acetylation. Science. 2001; 293:1653–7. [PubMed: 11533489]
38. Kanezaki R, et al. Transcription factor BACH1 is recruited to the nucleus by its novel alternative spliced isoform. J Biol Chem. 2001; 276:7278–84. [PubMed: 11069897]
39. Kim JY, Casaccia P. HDAC1 in axonal degeneration: A matter of subcellular localization. Cell Cycle. 2010; 9:3680–4. [PubMed: 20930523]
40. Lapalombella R, et al. Selective inhibitors of nuclear export show that CRM1/XPO1 is a target in chronic lymphocytic leukemia. Blood. 2012; 120:4621–34. [PubMed: 23034282]
41. Schmidt J, et al. Genome-wide studies in multiple myeloma identify XPO1/CRM1 as a critical target validated using the selective nuclear export inhibitor KPT-276. Leukemia. 201310.1038/leu.2013.172
42. Walker CJ, et al. Preclinical and clinical efficacy of XPO1/CRM1 inhibition by the karyopherin inhibitor KPT-330 in Ph+ leukemias. Blood. 2013; 122:3034–44. [PubMed: 23970380]
43. Tai YT, et al. CRM1 inhibition induces tumor cell cytotoxicity and impairs osteoclastogenesis in multiple myeloma: molecular mechanisms and therapeutic implications. Leukemia. 2014; 28:155–65. [PubMed: 23588715]
44. Huang WY, et al. Prognostic value of CRM1 in pancreas cancer. Clin Invest Med. 2009; 32:E315. [PubMed: 20003838]
45. Kojima K, et al. Prognostic impact and targeting of CRM1 in acute myeloid leukemia. Blood. 2013; 121:4166–74. [PubMed: 23564911]
46. Noske A, et al. Expression of the nuclear export protein chromosomal region maintenance/exportin 1/Xpo1 is a prognostic factor in human ovarian cancer. Cancer. 2008; 112:1733–43. [PubMed: 18306389]
47. Shen A, et al. Expression of CRM1 in human gliomas and its significance in p27 expression and clinical prognosis. Neurosurgery. 2009; 65:153–9. discussion 159-60. [PubMed: 19574837]
48. Wei Q, et al. EGFR, HER2 and HER3 expression in esophageal primary tumours and corresponding metastases. Int J Oncol. 2007; 31:493–9. [PubMed: 17671674]
49. Sato-Kuwabara Y, Neves JI, Fregnani JH, Sallum RA, Soares FA. Evaluation of gene amplification and protein expression of HER-2/neu in esophageal squamous cell carcinoma using Fluorescence in situ Hybridization (FISH) and immunohistochemistry. BMC Cancer. 2009; 9:6. [PubMed: 19128465]
50. Boone J, et al. mTOR in squamous cell carcinoma of the oesophagus: a potential target for molecular therapy? J Clin Pathol. 2008; 61:909–13. [PubMed: 18474542]
51. Akagi I, et al. Overexpression of PIK3CA is associated with lymph node metastasis in esophageal squamous cell carcinoma. Int J Oncol. 2009; 34:767–75. [PubMed: 19212681]
52. Garnett MJ, et al. Systematic identification of genomic markers of drug sensitivity in cancer cells. Nature. 2012; 483:570–5. [PubMed: 22460902]
53. Somaiah N, Simon GR. Molecular targeted agents and biologic therapies for lung cancer. J Thorac Oncol. 2011; 6:S1758–85. [PubMed: 22005529]
54. Su H, et al. Global gene expression profiling and validation in esophageal squamous cell carcinoma and its association with clinical phenotypes. Clin Cancer Res. 2011; 17:2955–66. [PubMed: 21385931]
55. Zhu YH, et al. Downregulation of the novel tumor suppressor DIRAS1 predicts poor prognosis in esophageal squamous cell carcinoma. Cancer Res. 73:2298–309. [PubMed: 23436800]

56. Lee DH, et al. Synergistic effect of low-dose cucurbitacin B and low-dose methotrexate for treatment of human osteosarcoma. Cancer Lett. 2011; 306:161–70. [PubMed: 21440986]
57. Sato Y, et al. Integrated molecular analysis of clear-cell renal cell carcinoma. Nat Genet. 2013; 45:860–7. [PubMed: 23797736]
58. Sakaguchi H, et al. Exome sequencing identifies secondary mutations of SETBP1 and JAK3 in juvenile myelomonocytic leukemia. Nat Genet. 2013; 45:937–41. [PubMed: 23832011]
59. Yoshida K, et al. Frequent pathway mutations of splicing machinery in myelodysplasia. Nature. 2011; 478:64–9. [PubMed: 21909114]
60. Lin DC, et al. Genomic and functional characterizations of phosphodiesterase subtype 4D in human cancers. Proc Natl Acad Sci U S A. 2013; 110:6109–14. [PubMed: 23536305]
61. Nannya Y, et al. A robust algorithm for copy number detection using high-density oligonucleotide single nucleotide polymorphism genotyping arrays. Cancer Res. 2005; 65:6071–9. [PubMed: 16024607]
62. Yamamoto G, et al. Highly sensitive method for genomewide detection of allelic composition in nonpaired, primary tumor specimens by use of affymetrix single-nucleotide-polymorphism genotyping microarrays. Am J Hum Genet. 2007; 81:114–26. [PubMed: 17564968]
63. Eden E, Navon R, Steinfeld I, Lipson D, Yakhini Z. GOrilla: a tool for discovery and visualization of enriched GO terms in ranked gene lists. BMC Bioinformatics. 2009; 10:48. [PubMed: 19192299]
64. Zhang B, Kirov S, Snoddy J. WebGestalt: an integrated system for exploring gene sets in various biological contexts. Nucleic Acids Res. 2005; 33:W741–8. [PubMed: 15980575]
65. Wang J, Duncan D, Shi Z, Zhang B. WEB-based GEne SeT AnaLysis Toolkit (WebGestalt): update 2013. Nucleic Acids Res. 2013; 41:W77–83. [PubMed: 23703215]

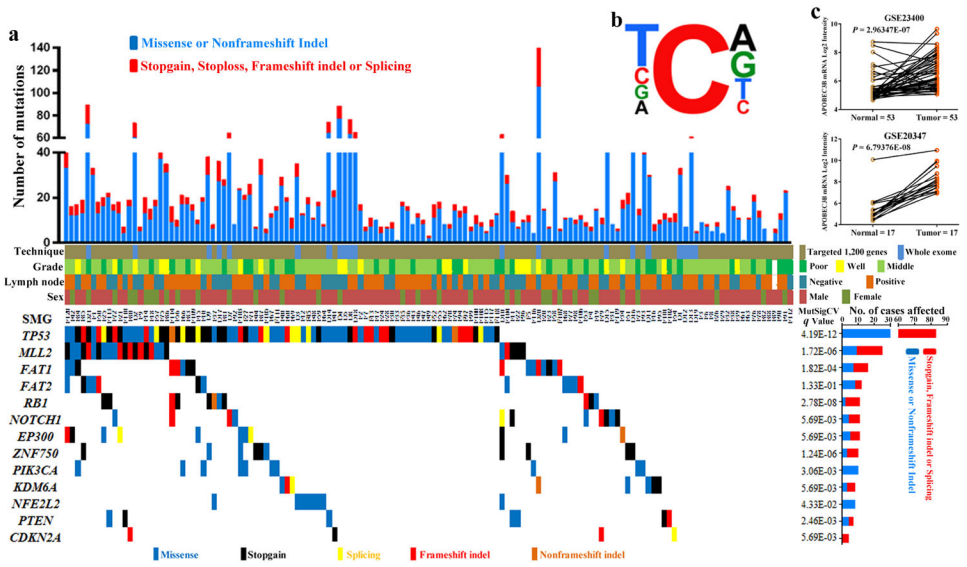

Figure 1. Mutation frequencies and signatures, and significantly mutated genes in 139 ESCCs

(a) The number of somatic mutations of each examined case (top), key clinical parameters (middle, see Supplementary Tables 2a and 2b), and the significantly mutated genes (SMG) colored by the type of mutations and their mutational frequency (bottom). Columns, examined cases; Rows, genes. (b) Trinucleotide contexts of mutations occurring at cytosine nucleotides in ESCC. Font size of the bases at the 5′ and 3′ positions are proportional to their frequencies (see Supplementary Fig. 3b). (c) APOBEC3B mRNA levels calculated from two datasets GSE20347[11] and GSE23400[54], both of which examined cDNA microarray from matched normal/tumor ESCC cases.

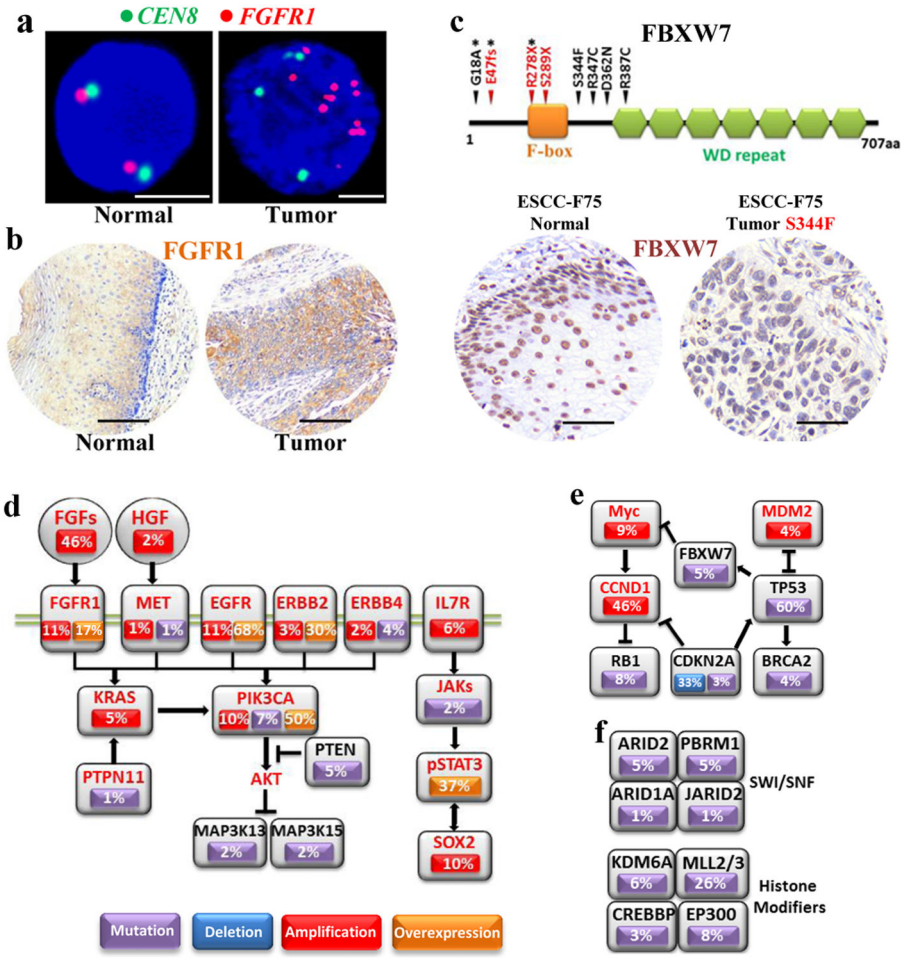

Figure 2. Dysregulated pathways in ESCC

(a) Representative FISH photos of an ESCC case with amplified *FGFR1*. Green signals label the centromere 8 probe (*CNE8*) and red signals label *FGFR1* gene probe. Scale bars, 5 μm. (b) Representative IHC photos of FGFR1 protein over-expression in ESCCs (Additional Cohort, 60 cases had matched adjacent normal epithelial tissues, see Supplementary Table 8a). Scale bars, 200 μm. (c) Top panel, schematics of protein alterations in FBXW7 caused by somatic mutations. Black, missense; red, stopgain (X) or frameshift indel (fs); *, discovered by Agrawal *et al.*[8]. Conserved domains were mapped from UniProt (See URL). Bottom panel, representative FBXW7 IHC results of an ESCC case carrying *FBXW7* mutations (Frequency and Additional Cohort, all cases had matched adjacent normal epithelial tissue, see Supplementary Table 8b). Scale bars, 100 μm. (d-f) Significantly dysregulated pathways colored by the type of alterations. Red font denotes a predicted activating alteration; black font denotes a predicted inactivating alteration. (d) RTK-MAPK-PI3K signaling; (e) G1-S cell cycle regulation; (f) Epigenetic modification.

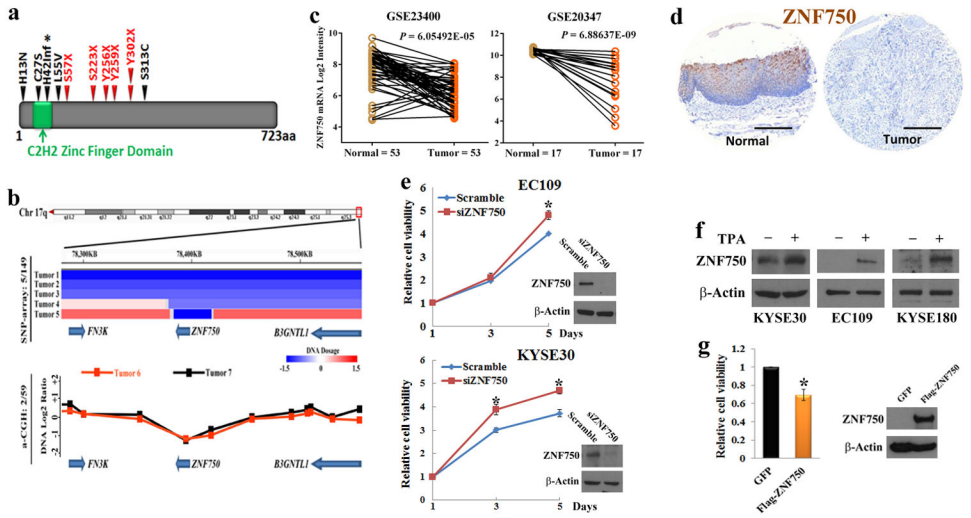

Figure 3. Indentification of ZNF750 as a novel recessive cancer gene in ESCC

(a) Schematics of protein alterations in ZNF750 caused by somatic mutations. Black, missense or inframe (inf); red, stopgain (X); *, discovered by Agrawal *et al.*[8]. Conserved domains were mapped from UniProt. (b) Top, IGV (Integrative Genomics Viewer) heatmap showing loss of *ZNF750* copy number identified from 149 ESCC SNP-array data; Bottom, segmentation map of two tumors with *ZNF750* deletions from 59 ESCCs examined with array-CGH. (c) ZNF750 mRNA levels calculated from GSE20347[11] and GSE23400[54]. (d) Representative IHC photos of ZNF750 protein expression in ESCCs (Additional Cohort, all cases had matched adjacent normal epithelial tissues, see Supplementary Table 8c). Scale bars, 400 μm. (e) Short-term cell proliferations assays of EC109 and KYSE30 cells transfected with either siRNAs against ZNF750 (si-ZNF750) or control siRNA (Scramble). Data represent mean ± SD; N = 3. (f) ESCC cells were treated with TPA (100nM) for 24 hours and lysates were subjected to WB analysis. (g) Under TPA (100nM) treatment, short-term cell proliferations assay of KYSE30 cells ectopically expressing either GFP or ZNF750 proteins. Data represent mean ± SD; N = 3. Blots of (e) and (g) showed the WB results of ZNF750 protein expression in indicated samples. β-Actin was examined as a loading control. *, $P < 0.05$.

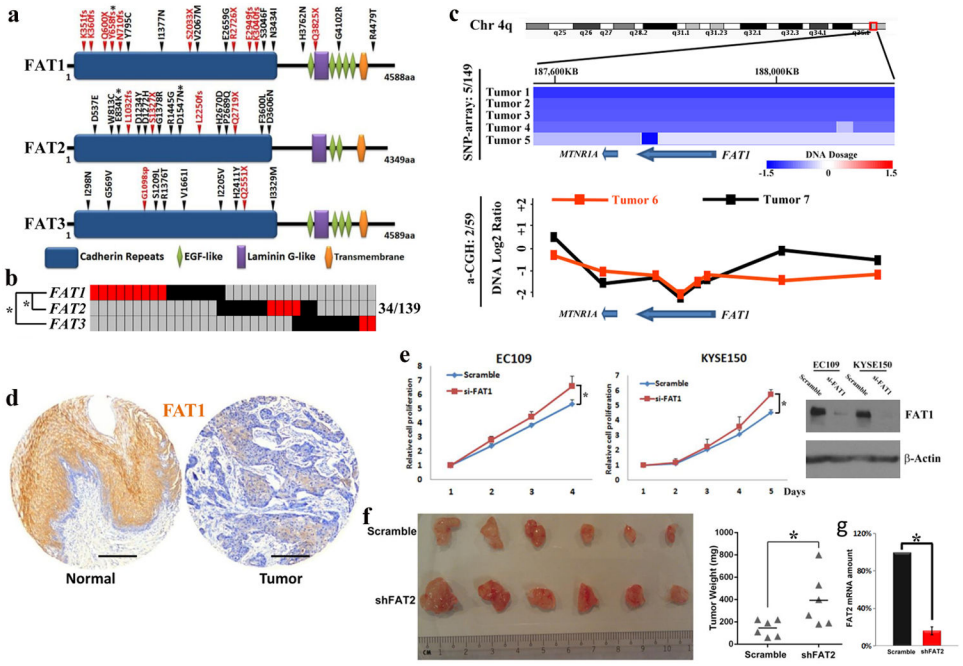

Figure 4. Inactivation of FAT1 through multiple mechanisms

(a) Schematics of protein alterations in FAT1, FAT2 and FAT3 caused by somatic mutations. Black, missense; red, stopgain (X), Splicing site (sp) or frameshift indel (fs); *, discovered by Agrawal *et al.*[8]. Conserved domains were mapped from UniProt. (b) Mutually exclusive analysis of *FAT1*, *FAT2* and *FAT3* mutations. Columns, examined cases; Rows, genes; Black, missense; red, stopgain, Splicing site or frameshift indel; *, P <0.01. (c) Top, IGV heatmap showing loss of *FAT1* copy number identifiedfrom 149 ESCC SNP-array data; Bottom, segmentation map of two tumors with *FAT1* deletions from 59 ESCC array-CGH data. (d) Representative IHC photos of FAT1 protein expression in ESCCs (Additional Cohort, all 18 cases had matched adjacent normal epithelial tissues, see Supplementary Table 8e). Scale bars, 400 μm. (e) Short-term cell proliferations were measured in EC109 and KYSE150 cells transfected with either siRNAs against FAT1 (si-FAT1) or control (Scramble). Value represent mean ± SD; N = 4. Blots showed the WB results of FAT1 protein level in indicated samples. β-Actin was detected as a loading control. (f) KYSE150 cells stably expressing either control shRNA (Scramble) or shRNA targeting FAT2 (shFAT2) were injected subcutaneously on the upper flanks of NOD/SCID mice. After 19 days, mice were sacrificed, and the tumors were analyzed. (g) Relative levels of mRNAs of FAT2 quantified with q-PCR in either Scramble or shFAT2 KYSE150 cells. Value represent mean ± SD; N = 3.*, P< 0.05.

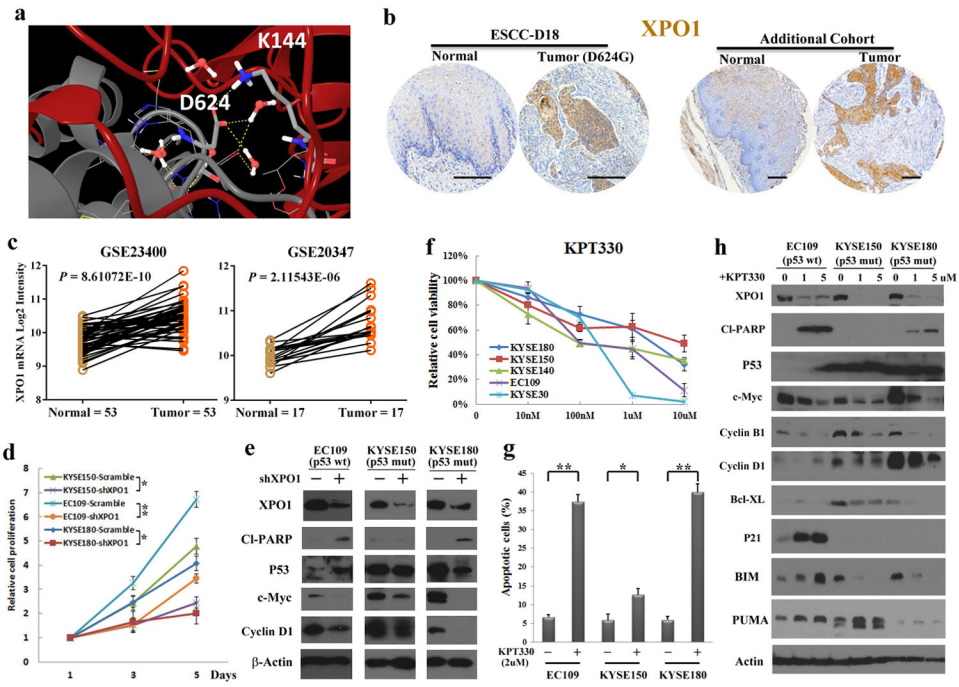

Figure 5. Targeting XPO1 in ESCC

(a) Crystal structural modeling of D624G mutation in XPO1 protein (grey ribbon) and its relationship with Snurportin (red ribbon). Dashed yellow lines represent hydrogen bonds. (b) Representative IHC photos of XPO1 protein expression in ESCCs (ESCC-D18 was from Discovery Cohort; the rest of the cases were from Additional Cohort, all cases had matched adjacent normal epithelial tissues, see Supplementary Table 8d). Scale bars, 200 μm. (c) XPO1 mRNA levels examined from GSE20347[11] and GSE23400[54]. (d) ESCC cells were infected with lentivirus encoding shRNA against either XPO1 (shXPO1) or control shRNA (Scramble), and their proliferation was measured, and (e) cell lysates were subjected to WB analysis with indicated antibodies. (f) ESCC cells were treated with KPT-330 at indicated concentrations for 72 hours, and cell proliferation and apoptosis (g) were measured, and (h) cell lysates were subjected to WB analysis with indicated antibodies. β-Actin was assayed as a loading control. Values of (d, f, g) represent mean ± SD. N = 4. **, $P < 0.01$; *, $P < 0.05$.